Clinical Cancer Research

Inhibition of SOAT1 Suppresses Glioblastoma Growth via Blocking SREBP-1–Mediated Lipogenesis

Feng Geng[1*], Xiang Cheng[1*], Xiaoning Wu[1], Ji Young Yoo[2], Chunming Cheng[1], Jeffrey Yunhua Guo[1], Xiaokui Mo[3], Peng Ru[1], Brian Hurwitz[2], Sung-Hak Kim[4], Jose Otero[5], Vinay Puduvalli[2], Etienne Lefai[6], Jianjie Ma[7], Ichiro Nakano[4], Craig Horbinski[8], Balveen Kaur[2], Arnab Chakravarti[1], and Deliang Guo[1]

Abstract

Purpose: Elevated lipogenesis regulated by sterol regulatory element-binding protein-1 (SREBP-1), a transcription factor playing a central role in lipid metabolism, is a novel characteristic of glioblastoma (GBM). The aim of this study was to identify effective approaches to suppress GBM growth by inhibition of SREBP-1. As SREBP activation is negatively regulated by endoplasmic reticulum (ER) cholesterol, we sought to determine whether suppression of sterol O-acyltransferase (SOAT), a key enzyme converting ER cholesterol to cholesterol esters (CE) to store in lipid droplets (LDs), effectively suppressed SREBP-1 and blocked GBM growth.

Experimental Design: The presence of LDs in glioma patient tumor tissues was analyzed using immunofluorescence, immunohistochemistry, and electronic microscopy. Western blotting and real-time PCR were performed to analyze protein levels and gene expression of GBM cells, respectively. Intracranial GBM xenografts were used to determine the effects of genetically silencing SOAT1 and SREBP-1 on tumor growth.

Results: Our study unraveled that cholesterol esterification and LD formation are signature of GBM, and human patients with glioma possess elevated LDs that correlate with GBM progression and poor survival. We revealed that SOAT1 is highly expressed in GBM and functions as a key player in controlling the cholesterol esterification and storage in GBM. Targeting SOAT1 suppresses GBM growth and prolongs survival in xenograft models via inhibition of SREBP-1–regulated lipid synthesis.

Conclusions: Cholesterol esterification and storage in LDs are novel characteristics of GBM, and inhibiting SOAT1 to block cholesterol esterification is a promising therapeutic strategy to treat GBM by suppressing SREBP-1. *Clin Cancer Res; 22(21); 5337–48. ©2016 AACR.*

Introduction

Emerging evidence demonstrates that lipid metabolism undergoes reprogramming in cancer cells (1–3). Identifying key aspects of lipid metabolism that are specifically engaged in tumorigenesis provides a new strategy to treat malignancies. However, our understanding of how lipid metabolism is regulated in tumor cells is incomplete. Our previous studies have revealed that sterol regulatory element-binding protein-1 (SREBP-1), a membrane-bound transcription factor with a central role in lipid metabolism, is highly activated in glioblastoma (GBM; refs. 4–7), a lethal primary brain tumor (8). Our studies also indicated that SREBP-1 may be a potential therapeutic target in malignancies (4, 5, 9).

There are three SREBP isoforms. SREBP-1a and -1c with a difference of around 20 amino acids in their N-terminus mainly regulate fatty acid synthesis, and SREBP-2 controls cholesterol synthesis (10–12). Under physiologic conditions, SREBP activity is tightly regulated by a negative feedback loop triggered by endoplasmic reticulum (ER) membrane cholesterol (2, 10). Recent reports show that even as low as 5% elevation of ER cholesterol significantly inhibits SREBP function (10, 13). Therefore, the approach to enhance ER cholesterol might be an effective therapeutic strategy to suppress GBM growth via inhibition of SREBP-1.

Interestingly, in addition to activating negative feedback loop to reduce lipid synthesis, cells have developed another layer of mechanism to prevent cholesterol accumulation in the ER membrane. When ER cholesterol increases, cells can esterify it with fatty acid to form cholesteryl esters (CE) and sequestrate them into lipid droplets (LDs). This happens through the activity of the ER-resident sterol O-acyltransferase (SOAT), also named as acyl-CoA:

[1]Department of Radiation Oncology, James Comprehensive Cancer Center & Arthur G James Cancer Hospital, The Ohio State Medical Center, Columbus, Ohio. [2]Department of Neurosurgery, James Comprehensive Cancer Center & Arthur G James Cancer Hospital, The Ohio State Medical Center, Columbus, Ohio. [3]Center for Biostatistics, Department of Biomedical Informatics, James Comprehensive Cancer Center & Arthur G James Cancer Hospital, The Ohio State Medical Center, Columbus, Ohio. [4]Department of Neurosurgery at University Alabama at Birmingham, Alabama. [5]Department of Pathology, James Comprehensive Cancer Center & Arthur G James Cancer Hospital, The Ohio State Medical Center, Columbus, Ohio. [6]CarMeN Laboratory, INSERM U1060, INRA 1397, Faculté de Médecine Lyon Sud, University de Lyon, Oullins, France. [7]Department of Surgery, James Comprehensive Cancer Center & Arthur G James Cancer Hospital, The Ohio State Medical Center, Columbus, Ohio. [8]Departments of Pathology and Neurosurgery at Northwestern University, Chicago, Illinois.

Note: Supplementary data for this article are available at Clinical Cancer Research Online (http://clincancerres.aacrjournals.org/).

F. Geng and X. Cheng contributed equally to this article.

Corresponding Author: Deliang Guo, OSU Comprehensive Cancer Center, 420 W 12th Avenue, Columbus, OH 43210. Phone: 614-366-3774; Fax: 614-247-1877; E-mail: deliang.guo@osumc.edu

doi: 10.1158/1078-0432.CCR-15-2973

Translational Relevance

Despite the use of advanced therapies, an average survival time of glioblastoma (GBM) patients has remained about 1 year over the past few decades. Our previous studies have revealed that lipid metabolism is reprogrammed and sterol regulatory element-binding protein-1 (SREBP-1) is highly upregulated in GBM to promote lipid synthesis and tumor growth. Here, we identified that blocking cholesterol esterification through inhibition of SOAT1 is a promising therapeutic strategy to target GBM via suppression of SREBP-1. Moreover, the discovery of cholesterol esterification and LDs uniquely formed in GBM tumor tissues provides an ideal metabolic target to specifically inhibit tumor cells while sparing normal brain tissues. Our study might shift the current paradigms in GBM treatment toward a new direction.

cholesterol acyltransferase (ACAT; refs. 14, 15). SOAT1 is ubiquitously expressed in most cell types and tissues, whereas SOAT2 is mainly present in fetal liver and intestine cells and rarely in other tissues (16–18).

Our previous studies revealed that SREBP-1 activity remains high in GBM cells, even though lipids like cholesterol are also high (4, 5, 7, 19). This raises the question as to how GBM cells could evade high levels of cholesterol-induced negative feedback inhibition and maintain SREBP activity (4, 5). A plausible explanation is that they might convert excess cholesterol to CE for storage in LDs, thus prevent the initiation of feedback inhibition on SREBP activation. In this study, we investigated whether LDs and CE are formed in glioma patient tumor tissues, and then determined whether blocking cholesterol esterification via inhibition of SOAT1 is an effective therapeutic approach to suppress SREBP-1 and inhibit GBM growth.

Materials and Methods

Reagents and chemicals

Antibodies for ACC (Acetyl-CoA Carboxylase; #3676), FASN (Fatty Acid Synthase; #3180) and SCD1 (Stearoyl-CoA Desaturase 1; #2438) were purchased from Cell Signaling Technology. Antibodies for β-actin (#A1978), paraformaldehyde (#P6148), glutaraldehyde solution (#G5882), G418 disulfate salt (#A1720), puromycin dihydrochloride (#P8833), Triton X-100 (#T8787), human EGF (#E9644), Heparin (#H3393), puromycin dihydrochloride (P8833), and Triton X-100 (#T8787) were purchased from Sigma. Cholesterol assay kit (A12216), Alexa Fluor 488 goat anti-rabbit IgG (#A-11034), Alexa Fluor 568 Goat Anti-Rabbit IgG (#A-11036), Neurobasal medium (#21103-049), and B-27 Supplement (50X)/minus vitamin A (#12587-010) were purchased from Life Technologies. Recombinant Human FGF basic 145 aa (#4114-TC-01M) was purchased from R&D. X-tremeGENE HP DNA Transfection Reagent (#06366236001) was purchased from Roche. Antibodies for LDLR (LDL Receptor; #ab30532) and TIP47 (Perilipin 3; #ab47638) were purchased from Abcam. Antibody for SREBP-1 (#557036) was purchased from BD. OCT (#23730571) and sucrose (#BP220212) were purchased from Fisher Scientific. Antibodies for SOAT1 (#sc-69836), PDI (Oxidoreductase-protein disulfide isomerase; #sc-30932, H-17), and SREBP-2 shRNA lentivirus (sc-36559-V) were purchased from Santa Cruz Biotechnology. Adenovirus expressing SREBP-1c (N-terminal fragment amino acid 1-461) was produced and amplified as described previously (20).

GBM patient biopsies

Glioma patient biopsies were obtained from the Department of Pathology at OSU Medical Center after surgery and fixed in 4% Paraformaldehyde for 24 hours. One half of biopsy was embedded in paraffin, and the second half was incubated with 30% sucrose for 24 hours, embedded in OCT. Cryosections derived from the latter were stained by BODIPY 493/503 (#D-3922; Life Technologies) or TIP47 antibody. The study of GBM patient tissues has been approved by OSU Institutional Human Care and Use Committee.

Glioma tissue microarray

Glioma tissue microarray (TMA), containing over 109 clinical patient samples from the University of Kentucky, was used to analyze TIP47 by immunofluorescent staining (see details in Fig. 1, Table 1). Two separate areas from each patient sample were included in this TMA. After antigen retrieval, sections were incubated with TIP47 antibody followed by fluorescence-labeled secondary antibody, and then photographed using a Zeiss LSM510 Meta confocal microscopy with 63x/1.4 NA oil objective. Five images in each core were captured, and 1-μm wide z-stacks acquired. TIP47 puncta were analyzed via ImageJ software (NIH) in a three-dimensional (3D) stack, and showing as average of TIP47 puncta/nucleus. Institutional Research Board approval was obtained at UK prior to study initiation.

Hematoxylin and eosin staining

Paraffin tissue sections were deparaffinized in xylene and rehydrated in degraded ethanol, respectively. After washing with dH2O, slides were stained with hematoxylin and eosin (H&E) solution in sequence followed by being washed with dH2O. Then, slides were dehydrated in degraded ethanol and immersed in xylene followed by mounting in Permount.

GBM cell lines

Human GBM cell lines U87, U87 stably expressing EGFRvIII, a constitutively active mutant of EGFR (U87/EGFRvIII; refs. 5, 21), T98, and U251 were cultured in DMEM (Corning Incorporated) supplemented with 5% FBS (Gemini Bio-Products) in a humidified atmosphere of 5% CO_2, 95% air at 37°C. GBM169, GBM88, and GBM30, primary GBM patient-derived cells described previously (22–24), were cultured in neurobasal medium supplemented with B27 (1x), Heparin (2 μg/mL), EGF (20 ng/mL), and FGF (20 ng/mL) in a humidified atmosphere of 5% CO_2, 95% air at 37°C. Human astrocyte cells were maintained in Geltrex matrix (#A1413202; Life Technologies) coated plates with DMEM supplemented with 1% of N-2 (#17502048; Life Technologies) and 10% of One Shot format FBS (#16000077; Life Technologies) at 37°C in a humidified atmosphere of 5% CO_2.

LD staining and quantification

LDs were stained by incubating cells with 0.5 μmol/L BODIPY 493/503 (Life Technologies) for 30 minutes and visualized by confocal microscope (Carl Zeiss LSM510 Meta; 63x/1.4 NA oil)

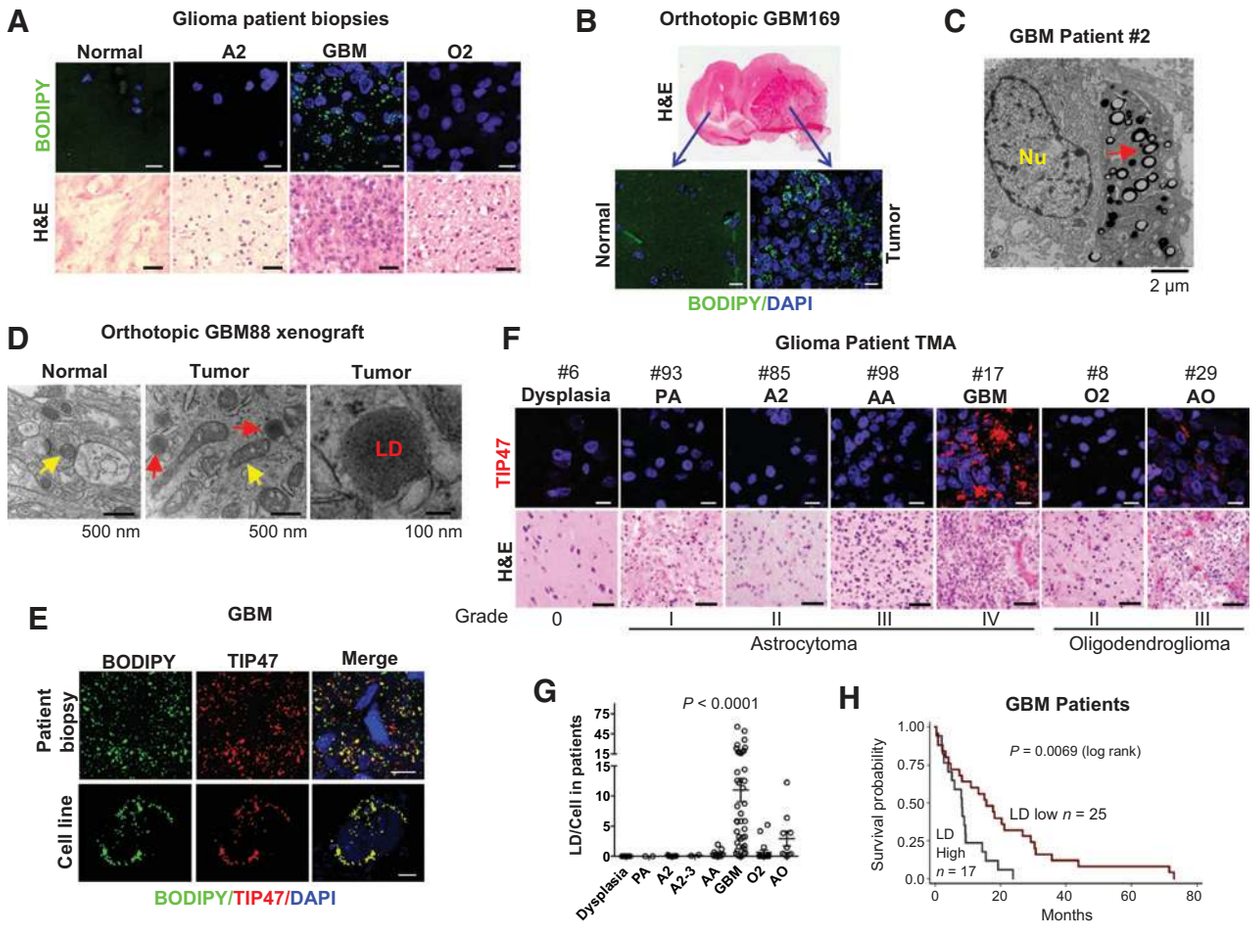

Figure 1.

Lipid droplets are signature of GBM and inversely correlate with patient survival. **A** and **B,** representative confocal microscopy images of cryosections of tissue biopsies from glioma patients (**A**) or from primary GBM169 orthotopic mouse model (**B**) stained with BODIPY 493/503 (green) and DAPI (blue; top plots). Tumor tissues were also stained by H&E (lower). A2: grade II astrocytoma. Scale bar, 10 μm for fluorescence imaging, 50 μm for H&E staining**. C** and **D,** representative electron micrographs of tumor tissues from GBM patients (**C**), or primary GBM88 orthotopic xenograft mouse model (**D**). **E,** representative fluorescent microscopy images of GBM patient tissues and U251 cells stained with BODIPY 493/503 (green), TIP47 antibody (red), and DAPI (blue). Scale bar, 10 μm. **F** and **G,** representative images of tissue samples from a TMA, containing low- to high-grade glioma patient samples (over 100 patients) and details, please see Supplementary Table S1, stained by TIP47 (red) and DAPI (blue; **F**). Data shown in **G** represent dot blot of quantification of LDs/cell in each sample in the TMA. LDs stained by TIP47 in each patient sample were quantified by ImageJ software and analyzed by GraphPad Prism and one-way ANOVA, $P < 0.0001$ (**G**). Scale bar, 10 μm for fluorescence imaging, 50 μm for H&E staining. AA, anaplastic astrocytoma (grade III). **H**, Kaplan–Meier analysis of overall survival of GBM patients stratified on the basis of LD number in each clinical sample. The mean of LD number in total GBM patients is 11 LDs/cell. Patients with more than this number were grouped as high LD group ($n = 17$), less than this number as low LD group ($n = 25$). GBM patient survival between low and high LDs was analyzed by log-rank test, $P = 0.0069$.

and 1-μm-wide z-stacks acquired. More than 30 cells in each group were analyzed, and particle numbers were quantified with ImageJ software (NIH) in a 3D stack (25).

Immunofluorescent microscopy

Cells were cultured and treated on glass cover slip, washed with PBS twice, and fixed with 4% paraformaldehyde/0.025% glutaraldehyde for 10 minutes followed by 5 minutes of permeabilization with 0.1%Triton X-100/PBS. After incubation with primary antibody overnight at 4°C, cells were incubated with fluorescence-labeled secondary antibody for 30 minutes at 37°C, then stained with 0.5 μmol/L BODIPY 493/503 for 30 minutes, and mounted with antifade reagent with DAPI (#P36935; Life Technologies) and visualized with confocal microscope.

Transmission electronic microscopy

Tissues were fixed in 2.5% glutaraldehyde/0.1 mol/L phosphate buffer, pH 7.4, for 10 minutes, and then further cut into pieces that are less than a 1-mm cube followed by fixation for overnight at 4°C. After fixation in 1% osmium tetroxide/phosphate buffer for 1 hour, tissue pieces were stained with 2% uranyl acetate/10% ethanol for 1 hour, followed by dehydration in upgraded ethanol. The tissues were finally embedded in Eponate 12 resin. Ultra-thin sections (70 nm) were produced on a Leica EM UC6 Ultramicrotome and stained with 2% uranyl acetate and Reynold's lead citrate. Transmission electronic microscopy (TEM) was performed on a FEI Tecnai G2 Spirit TEM at 80 kV. Images were captured using an AMT 2 × 2 digital camera. These experiments were performed at the OSU Microscopy Core Facility.

Table 1. Lipid droplets in glioma patient tissues and overall survival

ID#	Age at surgery	Gender	Initial diagnosis	LDs/cell	Ki67 positive%	OS (months)
6	51	F	**Dysplasia**	0.00	0.2	64.5
13	35	M	**Dysplasia**	0.00	0.3	35.2
24	41	M	**Dysplasia**	0.00	0.1	102.1
33	7	F	**Dysplasia**	0.00	0.6	50.1
42	36	M	**Dysplasia**	0.00	0.0	32.3
60	50	M	**Dysplasia**	0.00	0.5	20.2
70	34	M	**Dysplasia**	0.00	0.2	109.7
103	22	M	**Dysplasia**	0.00	0.1	31.4
107	26	M	**Dysplasia**	0.00	0.4	33.6
86	18	F	**PA**	0.00	0.7	90.5
93	15	M	**PA**	0.00	1.2	70.2
15	26	F	**A2**	0.23	0.5	42.5
57	24	M	**A2**	0.04	2.3	144.8
69	32	M	**A2**	0.00	1.7	63.5
77	29	M	**A2**	0.00	0.3	74.7
85	38	M	**A2**	0.00	0.2	82.6
88	41	M	**A2**	0.00	2.2	85.7
95	45	F	**A2**	0.00	2.5	20.3
101	73	M	**A2**	0.07	0.6	57.5
105	26	F	**A2**	0.00	1.8	6.8
7	27	M	**A2-3**	0.10	1.4	60.2
23	25	M	**A2-3**	0.23	2.3	41.0
10	59	M	**AA**	0.30	1.7	21.1
12	50	F	**AA**	1.21	1.0	82.3
41	49	F	**AA**	0.66	1.9	39.1
46	39	F	**AA**	0.00	10.2	41.6
59	48	F	**AA**	0.00	4.6	100.5
79	29	M	**AA**	0.17	9.8	26.5
98	36	M	**AA**	1.93	19.6	30.0
100	42	F	**AA**	0.01	2.0	26.8
104	23	M	**AA**	0.00	6.4	14.5
5	80	F	**GBM**	4.10	18.5	15.7
9	54	M	**GBM**	5.72	0.9	3.3
11	63	M	**GBM**	14.41	5.7	19.3
21	62	M	**GBM**	1.63	9.3	4.8
22	72	M	**GBM**	16.20	11.5	8.3
25	67	M	**GBM**	0.00	3.0	4.2
26	54	M	**GBM**	23.37	16.9	23.7
28	46	M	**GBM**	49.08	4.4	0.3
30	59	M	**GBM**	11.33	9.8	14.5
34	53	M	**GBM**	1.75	4.5	0.9
35	64	F	**GBM**	36.19	22.1	15.6
38	50	F	**GBM**	12.18	26.7	2.0
39	62	F	**GBM**	3.25	6.7	29.3
43	51	F	**GBM**	2.89	15.1	21.1
44	67	F	**GBM**	0.39	4.8	0.5
45	56	M	**GBM**	4.52	2.5	35.6
48	74	F	**GBM**	5.82	6.6	15.1
49	62	M	**GBM giant cell**	5.83	13.3	72.9
52	50	F	**GBM**	3.21	3.9	43.7
54	42	M	**GBM**	0.91	8.7	13.3
56	64	M	**GBM**	16.93	6.8	6.0
58	51	M	**GBM**	12.54	10.5	8.0
65	67	M	**GBM**	0.16	7.1	10.9
66	77	M	**GBM**	0.56	2.4	18.1
67	31	M	**GBM**	2.25	13.2	71.5
68	79	M	**GBM**	8.74	6.3	2.2
71	59	F	**GBM**	8.31	14.8	8.2
76	62	F	**GBM**	3.16	4.6	20.3
80	59	M	**GBM**	24.42	10.7	9.3
81	76	F	**GBM**	17.91	20.0	8.4
82	78	F	**GBM**	5.84	9.2	0.9
83	76	M	**GBM**	0.02	4.9	30.8
84	56	M	**GBM**	1.48	6.5	7.5
87	69	M	**GBM**	28.55	12.4	2.3
89	56	M	**GBM**	1.22	3.3	17.8

(Continued on the following page)

Table 1. Lipid droplets in glioma patient tissues and overall survival (Cont'd)

ID#	Age at surgery	Gender	Initial diagnosis	LDs/cell	Ki67 positive%	OS (months)
90	72	F	**GBM**	7.09	6.2	30.4
94	26	F	**GBM**	13.94	4.2	5.1
96	64	F	**GBM**	12.51	11.1	9.3
102	44	F	**GBM**	18.04	2.2	4.0
106	70	M	**GBM**	19.69	22.4	8.9
108	72	F	**GBM**	0.50	2.6	26.7
109	42	M	**GBM**	55.41	27.6	2.6
8	26	M	**O2**	0.00	0.5	49.4
14	37	M	**O2**	0.03	1.2	53.1
16	31	M	**O2**	1.50	3.0	91.7
18	35	M	**O2**	0.15	0.6	97.3
20	38	M	**O2**	0.02	0.7	30.6
32	25	M	**Recurrent O2**	5.22	1.8	82.9
36	38	M	**O2**	0.00	1.8	29.2
37	45	F	**O2-3**	0.00	2.6	66.6
50	27	F	**O2**	0.13	1.3	36.4
62	42	M	**O2**	0.00	1.9	64.4
63	31	F	**O2**	0.00	1.3	52.2
64	32	F	**O2**	0.00	1.6	60.8
72	58	M	**O2**	0.10	3.7	89.2
73	27	M	**O2**	0.08	1.4	98.2
91	40	F	**O2**	4.16	2.0	52.2
92	27	M	**O2**	0.00	1.8	83.3
99	65	M	**O2**	0.00	1.4	59.2
2	62	F	**AO**	3.91	4.8	60.8
4	56	F	**AO**	0.00	3.0	0.4
29	51	M	**AO**	12.24	18.6	4.5
31	32	M	**AO**	3.83	0.8	46.4
40	57	M	**AO**	6.39	6.7	15.1
47	32	F	**AO**	0.30	1.7	138.5
51	44	M	**AO**	0.40	2.5	15.3
53	49	M	**AO**	0.30	2.7	29.0
61	25	M	**Progressed to AO**	1.45	11.8	82.9
78	37	F	**Recurrent AO**	0.45	9.0	145.0

NOTE: Two separate areas from each patient in TMA were stained by TIP47 or Ki67 antibody and imaged by confocal or light microscopy. The number of LDs or Ki67-positive percentage was quantified by ImageJ software or Immunoratio, an online publicly available application (49). Five images were taken from each tissue and averaged. Control dysplasia is a disorganized piece of brain tissue that was causing seizures, but it is neither cancerous nor precancerous. The term "dysplasia" represents something very different in neuropathology compared with elsewhere in the body.

Abbreviations: PA, pilocytic astrocytoma; grade I astrocytoma; A2, grade II astrocytoma, AA; anaplastic astrocytoma, grade III astrocytoma; GBM, glioblastoma, grade IV astrocytoma; O2, grade II oligodendroglioma; AO, anaplastic oligodendroglioma, grade III; OS, overall survival.

Immunohistochemistry

Tissue sections were cut from paraffin blocks of GBM patient biopsies at 5 μm. The tissue slides were melted in oven at 60°C for 30 minutes, and then deparaffinized by xylenes three times for 5 minutes each followed by dipping in graded alcohols (100%, 95%, 80%, and 70%) three times for 2 minutes each. Slides were washed with distilled water (dH_2O) for 3 × 5 minutes, and then immersed in 3% hydrogen peroxide for 10 minutes followed by being washed thoroughly with dH_2O. Slides were transferred into preheated 0.01 mol/L citrate buffer (pH 6.0) in a steamer for 30 minutes, and then washed with dH_2O and PBS after cooling. Slides were blocked with 3% BSA/PBS for 1 hour at room temperature, and then incubated with primary antibody overnight at 4°C, followed by incubation with secondary antibody for 30 minutes at room temperature. After incubation with avidin–biotin ABC complex (#PK-4000; Vector labs) followed by PBS wash 3 × 5 minutes and staining with DAB solution (#SK-4105; Vector labs), slides were washed thoroughly with tap water, counterstained with hematoxylin (#H-3401; Vector labs), and dipped briefly in graded alcohols (70%, 80%, 95%, and 100%), in xylenes 2 × 5 minutes. Finally, slides were mounted and imaged.

Quantitative real-time PCR

Total RNA was isolated from cells with TRIZOL (#15596; Life Technologies) according to the manufacturer's instruction, and cDNA was synthesized with the iScript cDNA Synthesis Kit (#170-8891; Bio-Rad). Quantitative real-time PCR was performed with iQ SYBR Green Supermix (#170-8882; Bio-Rad) using the Applied Biosystems (ABI, it was merged into Life Technologies) 7900HT Real-Time PCR System. Results were normalized to the *36B4* housekeeping gene and calculated with the comparative method ($2^{-\Delta\Delta Ct}$). Primers for *36B4*: 5′- AATGGCAGCATCTACAACCC-3′ (forward) and 5′- TCGTTTGTACCCGTTGATGA-3′ (reverse). *SOAT1:* 5′-CCACTGGTCCAGATGAGTTTAG-3′ (forward) and 5′-GGGAACATGCAGAGTACCTTT-3′ (reverse).

Preparation of cell membrane fractions

Cell membranes were isolated as described previously (26). Briefly, cells were washed once with PBS, scraped into 1 mL PBS, and centrifuged at 1,000 × g for 5 minutes at 4°C. Cells were resuspended in an ice-cold buffer containing 10 mmol/L HEPES-KOH (pH 7.6), 10 mmol/L KCl, 1.5 mmol/L $MgCl_2$, 1 mmol/L sodium EDTA, 1 mmol/L sodium EGTA, 250 mmol/L sucrose and a mixture of protease inhibitors, 5 μg/mL pepstatin A (#P5318), 10

μg/mL leupeptin (#L2884), 0.5 mmol/L PMSF (#P7626), 1 mmol/L DTT (#43819), and 25 μg/mL ALLN (#A6185), which are all purchased from Sigma, for 30 minutes on ice. Extracts were then passed through a 22G x 1 1/2 inch needle 30 times and centrifuged at 890 × g at 4°C for 5 minutes to isolate nuclei. Supernatant was used for the separation of membrane fractions.

The supernatant from the original 890 × g spin was centrifuged at 20,000 × g for 20 minutes at 4°C. For subsequent Western blot analysis (for SOAT1 protein), the pellet was dissolved in 0.1 mL of SDS lysis buffer [10 mmol/L Tris-HCl pH 6.8, 100 mmol/L NaCl, 1% (v/v) SDS, 1 mmol/L sodium EDTA, and 1 mmol/L sodium EGTA] and designated "membrane fraction." The membrane fraction was incubated at 37°C for 30 minutes, and protein concentration was determined. Note that 1 μL 100x bromophenol blue solution was added before the samples were subjected to SDS-PAGE (26).

Western blot

Cultured cells were lysed using RIPA buffer (#NC9484499; Fisher Scientific) containing phosphatase inhibitor (#04906845001) and protease inhibitor cocktail (#11836170001; Roche) and 1 mmol/L phenylmethanesulfonyl fluoride. Equal amounts of protein extracts were separated by using 10% or 12% SDS-PAGE, and transferred onto a Hybond ECL nitrocellulose membranes (#RPN3032D; GE Healthcare). After blocking for 1 hour in a Tris-buffered saline containing 0.1% Tween 20 and 5% nonfat milk, the membranes were probed with various primary antibodies, followed by secondary antibodies conjugated to horseradish peroxidase. The immunoreactivity was revealed by use of an ECL kit (#RPN2106; Amersham Biosciences Co.).

Cholesterol esters measurement

Cells were washed with PBS twice and collected by scraping and centrifugation at 1,000 rpm for 10 minutes. The cell pellets were resuspended in Isopropanol/1% Triton X-100 for 1 hour at room temperature. After centrifugation at 12,000 rpm for 10 minutes, the supernatants were transferred into glass tubes and dried under nitrogen. Cholesterol and CE measurements were performed following the instruction manual of the cholesterol assay Kit (Life Technologies).

Lentiviral transduction

Mission pLKO.1-puro lentivirus vector containing SOAT1 shRNA (TRCN0000234512), SREBP-1 shRNA (TRCN0000414192), and the non-mammalian shRNA control (SHC002) were purchased from Sigma. 293FT cells were transfected with shRNA vector and packing plasmids pCMV-R8.74psPAX2 and the envelope plasmid pMD2.G using the polyethylenimine (#23966; Polysciences). The supernatant was collected at 48 hours and concentrated using the Lenti-X Concentrator (#631232; Clontech) according to the protocol. The lentiviral transduction was performed according to Sigma's MISSION protocol with polybrene (8 μg/mL; # H9268; Sigma).

Cell proliferation

A total of 1 to 2 × 10^4 cells were seeded in 12-well plates, and washed after 24 hours with PBS followed by changing to fresh medium with 5% FBS. Cells were counted at indicated time point using a hemocytometer, and dead cells were assessed using trypan blue exclusion assays (#15250-061; Life Technologies).

Intracranial mouse model and survival

Female athymic nude mice (6–8 weeks of age obtained from NCI) were used to generate intracranial xenograft models. A total of 1 × 10^5 cells in 4 μL of PBS were stereotactically implanted into mouse brain. Mice were then observed until they became moribund, at which point they were sacrificed. All animal procedures were approved by the Subcommittee on Research Animal Care at Ohio State University Medical Center.

Mice luminescent imaging

Mice implanted with cells expressing luciferase were injected with Luciferin (#122796; Perkin Elmer) solution (15 mg/mL in PBS, dose of 150 mg/kg) by an intraperitoneal route that is allowed to distribute in awake animals for about 5 to 15 minutes. The mice were placed into a clear Plexiglas anesthesia box (2.0%–3.0% isoflurane) that allows unimpeded visual monitoring of the animals; animals were then placed on nonfluorescent black paper on the imaging platform of an IVIS Lumina II to reduce background noise. The imaging chamber is continuously infused with 1% to 1.5% of isoflurane, and the imaging platform is heated at 37°C to keep the mice warm. Animals were imaged 10 minutes after Luciferin injection to ensure consistent photon flux (9). This imaging experiment was conducted at OSU Small Animal Imaging Core.

Lipid synthesis assay

Cells were seeded in a 12-well plate. After 24 hours, cells were changed to FBS-free medium containing 2 mmol/L glucose (#G8644; Sigma) and 2 mmol/L glutamine (#25030-081; Life Technologies) for 2 hours, then 0.5 μCi^{14}C-glucose (#NEC042V250UC; Perkin Elmer) was added into media for 2 hours. Cells were washed with PBS twice, and lipids were extracted with 0.5 mL of Hexane/Isopropanol (3:1) for 1 hour at room temperature and dried. The lipids were dissolved in 200 μL of chloroform and measured by Scintillation Counter (LS6500; Beckman Coulter, INC.).

Statistical analysis

Statistical analysis was performed with Excel and GraphPad Prism5. Cell proliferation, tumor volumes, and quantification of LDs in TMA were performed using the unpaired Student *t* test as well as by one-way ANOVA, as appropriate. The Kaplan–Meier plot was used for analysis of patient and mice overall survival (significance was analyzed by log-rank test). $P < 0.05$ was considered statistically significant.

Results

LDs are elevated in GBM and inversely correlate with patient survival

To determine whether cholesterol esterification and LDs exist in GBM, fluorescent lipid dye BODIPY 493/503 (27) was used to stain biopsy samples obtained from human glioma patients. We observed that LDs were highly prevalent in GBM patient tissues, but infrequently present in World Health Organization (WHO) grade II–III gliomas and undetectable in adjacent normal brain tissues (Fig. 1A). Elevated LDs were also observed in primary GBM169 orthotopic mouse glioma model, a GBM patient-derived xenograft model (Fig. 1B). The presence of LDs was confirmed by TEM in tumor tissues from GBM patients (Fig. 1C, red arrow) and in primary human GBM88 orthotopic tumors

implanted in nude mice (Fig. 1D, red arrow). In contrast, LD-like structures were not observed in normal brain tissues (Fig. 1D).

To examine the correlation between the prevalence of LDs and the grades of glioma tumors, we analyzed a TMA containing more than 100 glioma patient biopsy tissues (Table 1). TIP47, a protein marker of LD membrane (25), was shown to colocalize with BODIPY 493/503–stained LDs in GBM patient tumor tissues (Fig. 1E, top) and also in a variety of cancer cell lines (Fig. 1E, bottom; Supplementary Fig. S1). These data demonstrate that TIP47 staining detected LDs in GBMs and cell lines. We then quantified the number of TIP47-positive LDs in human patients with various grades of glioma (Fig. 1F and Table 1). Statistical analysis revealed that TIP47-stained LDs were predominantly present in GBM patient tissues (11 $\pm$ 12.8 LDs/cell), moderately present in anaplastic oligodendroglioma (AO, 2.9 $\pm$ 3.9), infrequently present in grade II oligodendroglioma (O2, 0.67 $\pm$ 1.57) and grade II (A2, 0.04 $\pm$ 0.08) to III astrocytoma (AA, 0.48 $\pm$ 0.68), and LDs were not detectable in grade I pilocytic astrocytoma (PA) and control dysplasia brain tissues ($P <$ 0.0001, one-way ANOVA; Fig. 1G and Table 1). By analyzing clinical data and LD numbers for each patient, we found that higher LD prevalence (i.e., more than the overall mean) inversely correlated with overall survival of GBM patients ($P = 0.0069$, log-rank; Fig. 1H). Moreover, we stained Ki67 in these patient tissues (Supplementary Fig. S2A and S2B; Table 1) and analyzed the correlation between Ki67-positive percentage and LD number in GBM patient tumor tissues. These data show a significant correlation between LD number and Ki67-positive percentage in GBM patients (Supplementary Fig. S2C). Collectively, our data demonstrate that LDs are a new feature of GBM and correlate with its aggressive behavior.

Inhibition of cholesterol esterification via targeting SOAT1 blocks LD formation

Because CE is a major component of LDs (14) and SOATs are essential enzymes for CE synthesis (28), we sought to determine SOAT protein level and its correlation with LD formation in glioma patient tumor tissues. As shown in Fig. 2A, SOAT1, examined by immunohistochemistry (IHC; bottom), was highly expressed in tumor tissues from GBM patients, but much lower in low-grade glioma patient samples and normal brain tissues (Supplementary Fig. S3A), which were correlated with the prevalence of LDs in glioma patient tissues (middle). In contrast, SOAT2 was not detectable in GBM patient tumor tissues (Supplementary Fig. S3B). These data are consistent with previous reports from other groups (16–18), showing that SOAT2 is highly expressed only in fetal liver and intestine, and modestly in the HepG2 cell line, but rarely in other tissues. We compared the gene expression levels of *SOAT1* and *SOAT2* and SOAT2 protein expression in HepG2 and GBM cell lines by using real-time PCR analysis and Western blot. As shown in Supplementary Fig. S3C and S3D, the expression level of *SOAT1* was similar to HepG2 and GBM cell lines. However, *SOAT2* level was extremely lower in GBM cells, and its protein was not detectable in GBM cells. Moreover, we analyzed *SOAT1* and *SOAT2* gene expression in ciBioPortal and The Cancer Genome Atlas database in glioma patients and across different cancer types (29, 30). These data show that *SOAT1* is highly expressed in GBM and all cancer types. In contrast, *SOAT2* is rarely expressed in GBM and the majority of cancer types, except liver cancer (high expression) and testicular germ cell cancer (modest expression; Supplementary Fig. S3E and S3F). Thus, SOAT1, but not SOAT2, may play a central role in CE synthesis and LD formation in GBM tumor tissues.

We then examined whether SOAT1 controls cholesterol esterification and storage in GBM cells. We used shRNA lentivirus to knock down the expression of SOAT1 in multiple GBM cell lines and primary GBM30 cells. As shown in Fig. 2B and Supplementary Fig. S4A, both mRNA and protein of SOAT1 were markedly reduced after knockdown for 48 hours. Confocal imaging revealed that knockdown of SOAT1 markedly reduced CE levels and diminished LD formation in GBM cells (Fig. 2C and Supplementary Fig. S4B). Likewise, pharmacologic inhibition of SOAT1 by avasimibe, a clinically tested SOAT inhibitor (31–33), also markedly reduced CE levels and blocked LD formation in GBM cells (Fig. 2D and Supplementary Fig. S4C). Interestingly, cellular cholesterol levels were not significantly enhanced by knockdown of SOAT1 or avasimibe treatment (Supplementary Fig. S5), suggesting the tight control of cholesterol homeostasis via negative feedback loop (13). Taken together, our data strongly demonstrate that SOAT1 plays a critical role in regulating CE synthesis and LD formation in GBM.

Inhibition of SOAT1 suppresses GBM growth via blocking SREBP-1–regulated fatty acid synthesis pathway

We then asked whether inhibition of cholesterol esterification, via inhibition of SOAT1, affected tumor growth. We found that pharmacologic inhibition of SOAT by avasimibe markedly inhibited GBM cell growth in a dose-dependent manner, but no obvious inhibitory effects in normal human astrocyte (Fig. 3A), consistent with the prior reports in cell culture (34, 35). To further verify that SOAT1 plays a key role in GBM growth, we knocked down SOAT1 and measured cell viability in various GBM cell lines. The U87/EGFRvIII and primary GBM30 cells constitutively expressing luciferase were used to monitor orthotopic xenograft growth by using luminescent imaging (36). Consistent with higher expression of SOAT1 in GBM (Fig. 2A), the data show that knockdown of SOAT1 significantly reduced GBM cell viability *in vitro* (Fig. 3B), markedly slowed down orthotopic U87/EGFRvIII and GBM30 tumor growth (Fig. 3C), and significantly prolonged the overall survival of intracranial GBM-bearing mice in comparison with control knockdown (Fig. 3D). Collectively, these data demonstrate that SOAT1 is a potentially viable therapeutic target in GBM.

Because inhibition of cholesterol esterification may trigger feedback inhibition of SREBP (11, 13), we examined whether targeting SOAT1 would affect SREBP activity in GBM cells. Western blot analysis revealed that knockdown of SOAT1 in multiple GBM cells led to significant inhibition of SREBP-1 activation, as reflected by the diminished appearance of the N-terminal cleavage product of SREBP-1 (Fig. 3E and Supplementary Fig. S6A). Moreover, SREBP-1–regulated downstream lipogenesis enzymes, ACC, FASN, and SCD1 (11, 12, 37, 38), were all reduced in cells with knockdown of SOAT1 (Fig. 3E and Supplementary Fig. S6A).

To directly test if knockdown of SOAT1 reduced SREBP-1–regulated *de novo* lipid synthesis, we performed a pulse chase labeled experiment. ^{14}C-labeled glucose was added to the cell medium, and the amount of newly synthesized ^{14}C-labeled lipids in U87/EGFRvIII cells were measured. As shown in Fig. 3F, knockdown of SOAT1 significantly reduced *de novo* lipid synthesis. We then determined whether knockdown of SOAT1-mediated inhibition of GBM tumor growth (Fig. 3B–D) was due to the

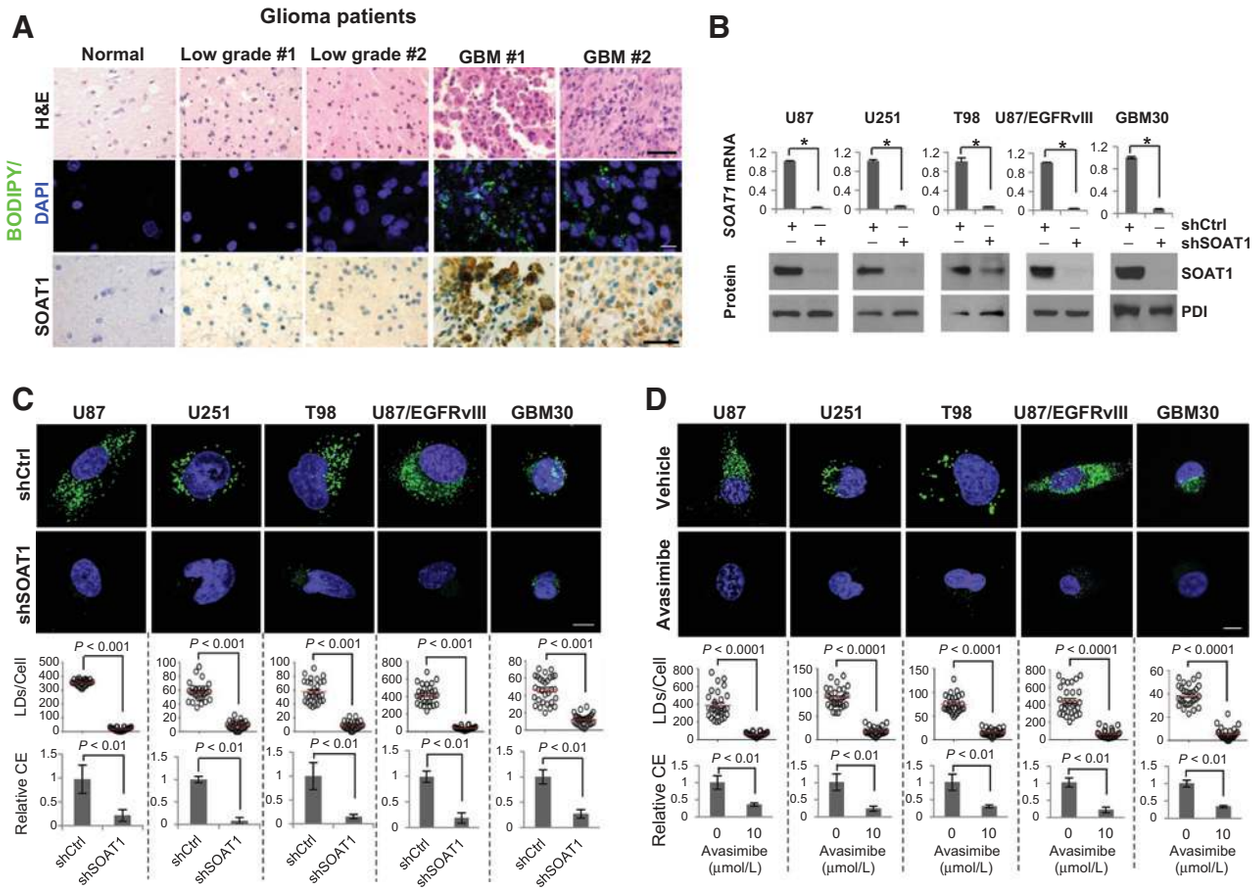

Figure 2.

Inhibition of cholesterol esterification via targeting SOAT1 blocks LD formation. **A,** human tissues from glioma patients were stained by H&E (top), BODIPY 493/503 (green)/DAPI (blue; middle), or IHC via using SOAT1 antibody (bottom). Scale bar, 50 μm for H&E (top) and IHC staining (bottom), 10 μm for fluorescence imaging (middle). **B**, relative *SOAT1* gene expression analyzed by real-time RT-PCR (top) and its protein level analyzed by Western blot (bottom) in different GBM cell lines and GBM30, primary GBM patient-derived cells, infected with shRNA-expressing lentivirus against SOAT1 for 48 hours. Significance for gene expression (top) was determined by an unpaired Student *t* test (mean ± SD, $n = 3$). *, $P < 0.001$. SOAT1 protein was detected from membrane extracts of GBM cells (please see details in Materials and Methods). Protein disulfide-isomerase (PDI), an ER-resident protein, was used as internal control. **C** and **D,** top plots show representative live confocal microscopy images of indicated GBM cells knocked down for SOAT1 (48 hours; **C**) or treated with SOAT inhibitor avasimibe (10 μmol/L) for 24 hours (**D**), after staining by BODIPY 493/503 (green) and Hoechst 33342 (nuclear, blue). Scale bar, 10 μm. Bottom represents quantification of LDs/cell quantified by ImageJ software in over 30 cells (mean ± SEM, $n = 30$), and relative CE levels measured by CE measuring kit (mean ± SD, $n = 3$), respectively. Significance was determined by an unpaired Student *t* test.

suppression of SREBP-1–regulated lipid synthesis. Palmitate (PA) and oleic acid (OA), the major end products of *de novo* fatty acid synthesis regulated by FASN and SCD1, were added to SOAT1 knockdown cells. The data showed that the addition of PA/OA mixture prevented SOAT1 knockdown-induced GBM cell death (Fig. 3G).

We also performed pharmacologic studies with treatment of multiple GBM cells with avasimibe. As shown in Fig. 3H and Supplementary Fig. S6B, avasimibe inhibition of SOAT reduced SREBP-1 cleavage and inhibited the expression of its targets (ACC, FASN, and SCD1), similar to that observed with knockdown of SOAT1 (Fig. 3E). Moreover, treatment of GBM cells with avasimibe also reduced *de novo* lipid synthesis (Fig. 3I), and addition of PA/OA significantly reduced avasimibe treatment-induced cell death (Fig. 3J). We then applied an adenovirus-mediated expression of the N-terminal form of SREBP-1c (Ad-nSREBP-1c), to determine whether SREBP-1 could also rescue SOAT1 inhibition-induced cell death. As shown in Fig. 3K, expression of active SREBP-1c in U87/EGFRvIII cells markedly enhanced the expression of fatty acid synthesis enzymes, ACC, FASN, and SCD1, and significantly reduced avasimibe treatment-induced cell death (Fig. 3L). We noticed that the levels of LDLR and fluorescent Dil-LDL uptake were not affected by silencing of *SOAT1* gene in GBM cells (Supplementary Fig. S7). Taken together, these data demonstrate that SOAT1 inhibition leads to suppression of SREBP-1–regulated fatty acid synthesis, in turn causing GBM cell death.

Silencing of SREBP-1 suppresses GBM growth

Although our data presented in Fig. 3 support a role for SREBP-1–mediated *de novo* lipid synthesis in controlling the growth of GBM, a direct test for the function of SREBP-1 in GBM progression is shown in Fig. 4. We employed shRNA to silence SREBP-1

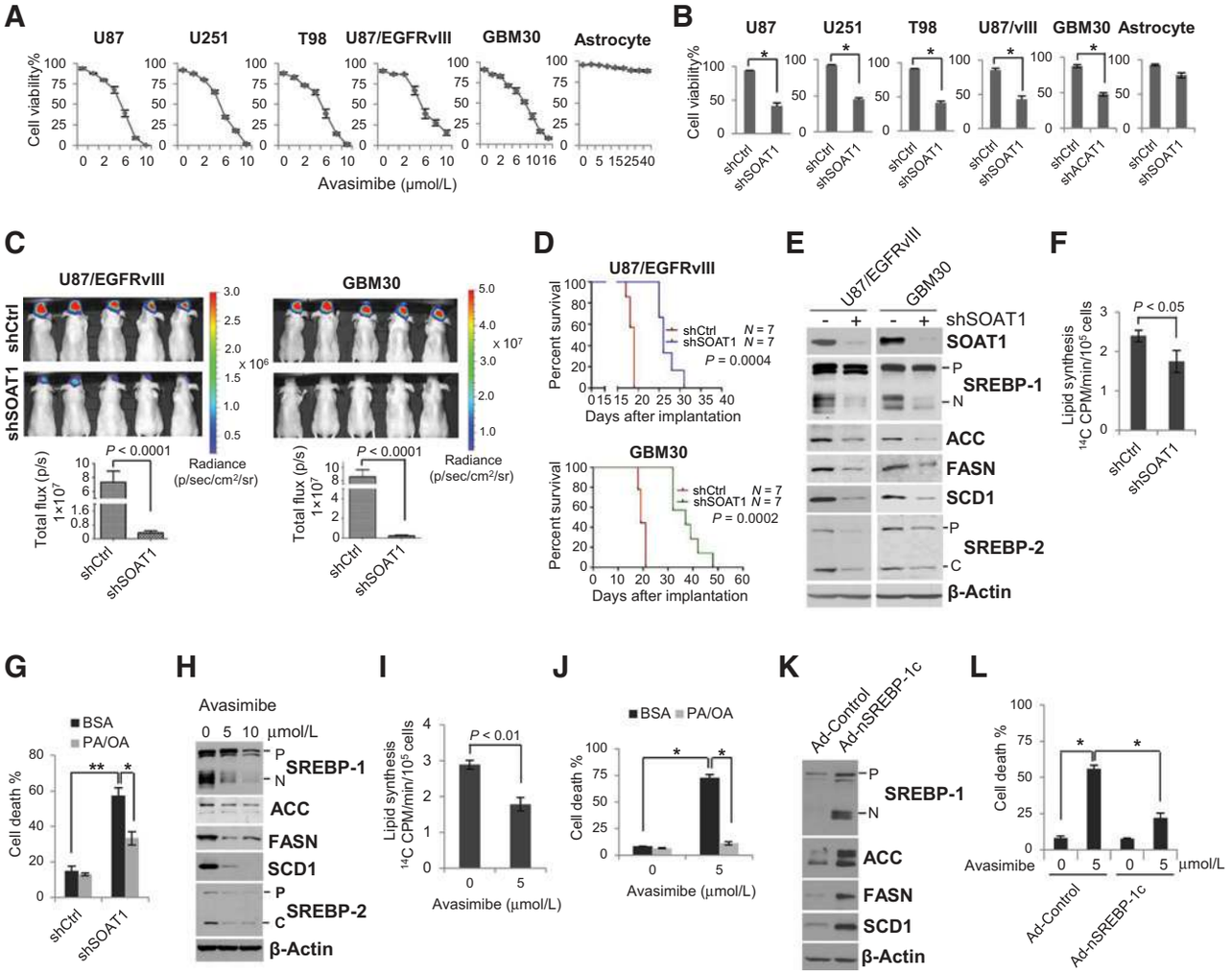

Figure 3.

Inhibition of SOAT1 suppresses GBM growth via blocking SREBP-1–regulated fatty acid synthesis. **A** and **B,** GBM cells or normal astrocyte were treated with SOAT inhibitor avasimibe at different doses for 3 days (**A**) or knockdown of SOAT1 for 5 days (**B**), cell number were then counted after trypan blue staining, and cell viability was analyzed via live cells dividing total cell numbers (mean ± SD, $n = 3$). Significance was determined by an unpaired Student t test. *, $P < 0.001$. **C,** *in vivo* luminescent imaging of mice bearing intracranial U87/EGFRvIII-luciferase or GBM30-luciferase cells in athymic nude mice on day 15 after intracranially implanting the indicated GBM cells (top). Bottom plot shows the quantification of luminescence signal intensity from intracranial tumor on day 15 after implanting the indicated GBM cells. Statistical significance was analyzed by an unpaired Student t test (mean ± SEM, $n = 7$). **D,** Kaplan–Meier analysis shows the overall survival of U87/EGFRvIII- or GBM30-bearing orthotopic mouse with shSOAT1 knockdown in comparison with scramble shRNA control and analyzed by log-rank test ($n = 7$). **E,** Western blot analysis of total cell lysates from U87/EGFRvIII or primary GBM30 cells after knockdown of SOAT1 for 48 hours. P: SREBP-1 or SREBP-2 precursor, which is full length of SREBP protein; N: N-terminal cleavage form of SREBP-1 which translocates into nuclei acting as transcription factor; C: C-terminal cleavage form of SREBP-2 which remains in cytoplasmic. **F,** ^{14}C-labeled glucose was added to U87/EGFRvIII cells for 2 hours after knockdown of SOAT1 for 48 hours, lipids were then extracted and measured by scintillation counter. Significance was determined by an unpaired Student t test (mean ± SD, $n = 3$). **G,** the mixture of PA (10 μmol/L) and OA (15 μmol/L), which were conjugated with lipid-free BSA, was added into U87/EGFRvIII cells 24 hours after knockdown of SOAT1, and cell death percentage was analyzed by counting live and dead cell number after trypan blue staining at day 5. Significance was determined by an unpaired Student t test (mean ± SD, $n = 3$). *, $P < 0.01$; **, $P < 0.001$. **H,** Western blot analysis of total cell lysates from U87/EGFRvIII cells after avasimibe treatment for 24 hours. The abbreviations of P, N, and C are same as **E**. **I,** ^{14}C-labeled glucose was added into U87/EGFRvIII cells for 2 hours after avasimibe treatment for 24 hours, lipids were then extracted and measured by scintillation counter. Significance was determined by an unpaired Student t test (mean ± SD, $n = 3$). **J,** U87/EGFRvIII cells were treated with avasimibe (5 μmol/L) with/without addition of PA (10 μmol/L) and OA (15 μmol/L) for 3 days, and cell numbers were counted after trypan blue staining. Significance was determined by an unpaired Student t test (mean ± SD, $n = 3$). *, $P < 0.001$. **K,** Western blot analysis of the total cell lysates from U87/EGFRvIII cells overexpressing adenovirus-mediated SREBP-1c N-terminal fragment (aa 1-461, Ad-nSREBP-1c) for 24 hours. **L,** U87/EGFRvIII cells were infected with Ad-control or Ad-nSREBP-1c virus for 24 hours, and then treated with avasimibe (5 μmol/L) for 48 hours, cell numbers were counted after trypan blue staining. Significance was determined by an unpaired Student t test (mean ± SD, $n = 3$). *, $P < 0.001$.

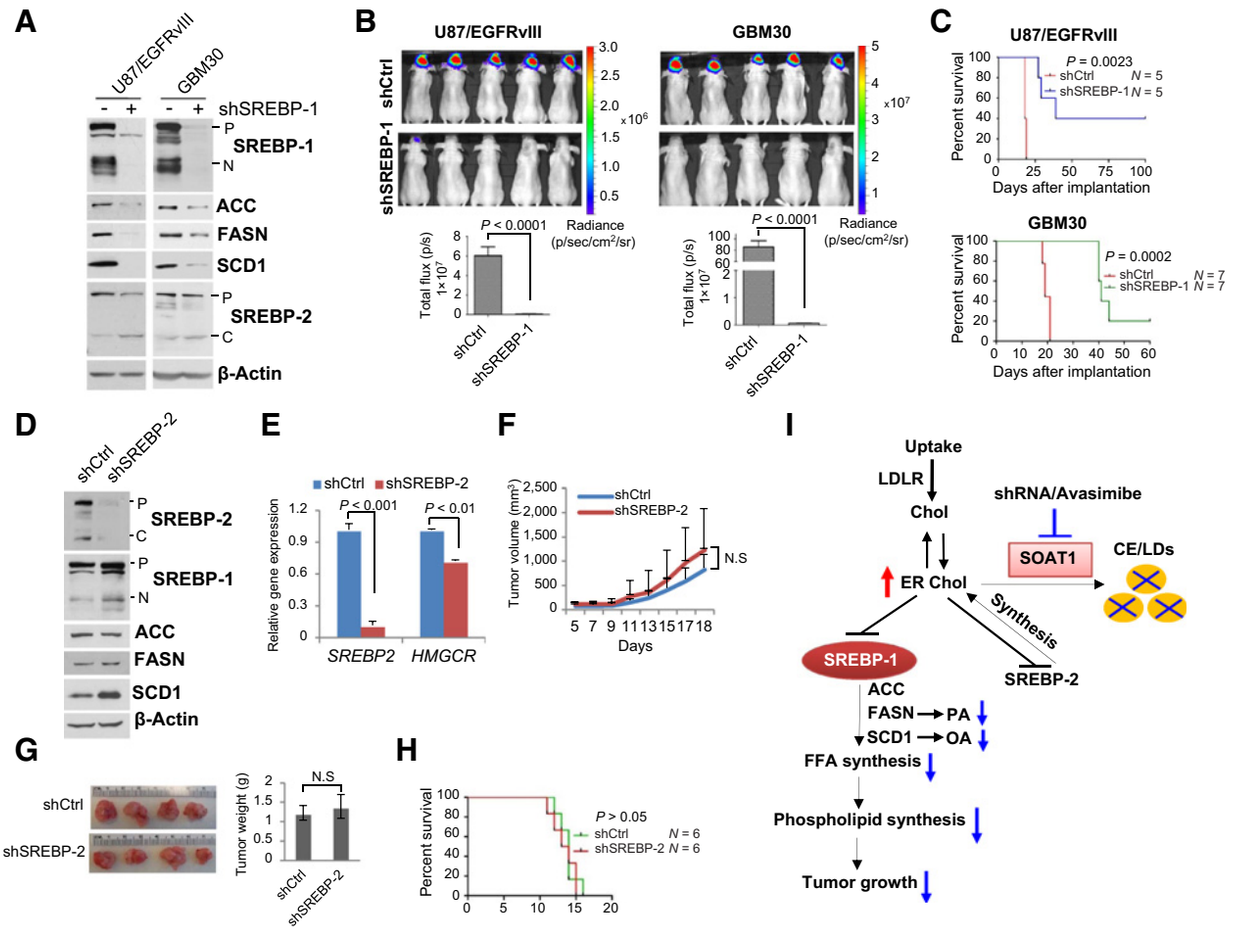

Figure 4.

Inhibition of SREBP-1 suppresses GBM tumor growth. **A–C,** U87/EGFRvIII or primary GBM30 cells stably expressing luciferase were infected with shRNA-expressing lentivirus for 48 hours to knockdown the expression of SREBP-1. Western blotting was performed to analyze the total cell lysates by using indicated antibodies (**A**). Cells were analyzed for *in vivo* growth after intracranial implantation into nu/nu mice (1×10^5 cells/mouse). Luminescent images were taken on day 15 (**B**, top), and luminescence signal intensity in mice was quantified (mean ± SEM, $n = 7$; **B**, bottom). Mouse overall survival was analyzed by Kaplan–Meier plot (**C**). Statistical significance was analyzed by log-rank test. $P = 0.0023$. **D** and **E,** Western blot analysis of total cell lysates (**D**) or real-time PCR analysis (**E**) of U87/EGFRvIII cells after silencing of SREBP-2 using shRNA lentivirus in comparison with control virus infection (shCtrl). *HMG-CoA reductase* (*HMGCR*), a downstream target of SREBP-2, was also analyzed by real-time PCR (**E**). **F** and **G,** 1×10^6 U87/EGFRvIII cells stably expressing shSREBP-2 or shControl were implanted into mouse flanks. Tumor size was measured every other day (**F**) and was imaged and weighted after isolation from mouse flanks on day 18 (**G**). Statistical significance was analyzed by an unpaired Student *t* test (mean ± SEM, $n = 6$). N.S: no significant difference. **H,** 1×10^5 U87/EGFRvIII cells stably expressing shControl (shCtrl) or shSREBP-2 were implanted into mouse intracranially, and mouse overall survival was analyzed by Kaplan–Meier plot and log-rank test. $P > 0.05$ between two groups. **I,** schematic model illustrates the functional interplay between SOAT1, LDs, and SREBP-1 in lipid metabolism and tumorigenesis of GBM. Increased CE and LDs are signatures of GBM. Inhibition of SOAT1 blocks CE synthesis and LD formation. This leads to an accumulation of cholesterol in the ER membrane, and consequently triggers feedback inhibition on SREBP-1 and SREBP-2 function. Suppression of SREBP-1 by targeting SOAT1 leads to the reduction of fatty acid synthesis (PA and OA) and phospholipid formation that restrains GBM tumor growth. Chol, cholesterol; FFA, free fatty acids.

expression in cultured U87/EGFRvIII and GBM30 cells (Fig. 4A). As expected, knockdown of SREBP-1 led to reduced expression of its downstream enzymes, ACC, FASN, and SCD1. After silencing of SREBP-1, GBM cells were implanted into the mouse brain. As shown in Fig. 4B, reduced brain tumor formation and growth were clearly observed with GBM cells after knockdown of SREBP-1 by luminescent imaging, as well as increased overall survival (Fig. 4C). These results are consistent with previous studies showing that knockdown of SREBP-1 reduced tumor growth in mouse flank (39, 40).

While studying shRNA-silencing and pharmacologic inhibition of SOAT1 in GBM cells, we noticed that cells with inhibition of SOAT1 also displayed reduced cleavage product for SREBP-2 (Fig. 3E and H). This raised the possibility that reduction of SREBP-2 might potentially contribute to SOAT1 inhibition-mediated suppression of GBM. We thus used shRNA to silence the expression of SREBP-2 in U87/EGFRvIII cells (Fig. 4D and E). As shown in Fig. 4F–H, mice implanted with control GBM cells and shSREBP-2 cells in the flank or intracranially showed similar patterns of tumor growth and overall survival. Interestingly, Western blot analysis showed that knockdown of SREBP-2 modestly enhanced SREBP-1 cleavage and SCD1 protein levels (Fig. 4D), which may abrogate the antitumor effects of silencing SREBP-2 expression. Thus, the reduced lipogenesis

associated with tumor suppression of GBM reflects the involvement of SREBP-1, but not SREBP-2.

Discussion

In this study, we provided strong evidence that LDs are present in GBM, and found that LD prevalence inversely correlated with GBM patient survival. We also found that inhibition of cholesterol esterification via targeting SOAT1 blocked LD formation and suppressed GBM growth by inhibiting SREBP-1–regulated lipogenesis. Our data provide the first evidence that targeting SOAT1 is an effective means to treat GBM via inhibition of SREBP-1.

GBM is one of the most difficult cancers to treat (8), and a metabolically active tumor that exhibits elevated glycolysis, exaggerated lipogenesis, and enhanced LDL-cholesterol uptake, which work together to increase lipid levels in tumor cells to promote their rapid growth (4, 5, 7, 9, 41, 42). In normal cells, cholesterol is strictly maintained at relatively stable levels (13); when ER cholesterol level increases, it triggers a negative feedback loop to inhibit its *de novo* synthesis (10, 11). Our present study shows that GBM cells convert excess cholesterol to CE that is stored in LDs, to prevent cholesterol accumulation in the ER membrane and avoid inducing feedback inhibition on SREBPs and tumor growth (6, 10).

Although the ER is responsible for regulation of cholesterol synthesis and storage, its cholesterol concentration is maintained at a very low level, comprising only 3% to 6% of ER lipids (43–45). Even just a 5% increase in ER cholesterol is sufficient to block SREBPs from trafficking to the Golgi and being activated (13). Thus, raising ER cholesterol could inhibit SREBP-1, impair lipogenesis, and block cancer growth. Although SREBP-1 was discovered over 20 years ago (10), development of clinically viable pharmacologic SREBP-1 inhibitors has not been successful. For the first time, we showed that forcing cholesterol to accumulate in the ER, via SOAT1 inhibition, achieves the same objectives as direct SREBP-1 inhibition. Because SOAT1 is a much more viable pharmacologic target than SREBP-1, with an inhibitor that has already been tested in clinical trials on cardiovascular patients (33), this can be quickly translated into clinical trials for cancer patients. SOAT1 inhibition might be especially effective against tumors that contain large amount of CE and LDs, such as GBMs.

Lipids stored in LDs could potentially be mobilized when cancer cells are challenged by a harsh microenvironment (46–48). Further work is necessary to examine how tumor cells mobilize and utilize lipids stored in LDs. The current study advances our understanding of lipid metabolism in cancer, and highlights the therapeutic potential of LDs in cancer therapy. Therefore, further exploring the role of LDs in malignant tumors, and developing optimal targeting strategies, might shift the current paradigms in cancer treatment in an entirely new direction.

Disclosure of Potential Conflicts of Interest

No potential conflicts of interest were disclosed.

Authors' Contributions

Conception and design: F. Geng, X. Cheng, D. Guo

Development of methodology: F. Geng, X. Cheng, J.Y. Yoo, S. Kim, I. Nakano, C. Horbinski, D. Guo

Acquisition of data (provided animals, acquired and managed patients, provided facilities, etc.): F. Geng, X. Cheng, X. Wu, C. Cheng, J.Y. Guo, B. Hurwitz, E. Lefai, C. Horbinski, B. Kaur, D. Guo

Analysis and interpretation of data (e.g., statistical analysis, biostatistics, computational analysis): F. Geng, X. Cheng, X. Mo, P. Ru, V. Puduvalli, C. Horbinski, A. Chakravarti, D. Guo

Writing, review, and/or revision of the manuscript: F. Geng, X. Cheng, X. Mo, J. Otero, J. Ma, C. Horbinski, A. Chakravarti, D. Guo

Administrative, technical, or material support (i.e., reporting or organizing data, constructing databases): F. Geng, X. Cheng, X. Mo, J. Otero, J. Ma, C. Horbinski, A. Chakravarti, D. Guo

Study supervision: D. Guo

Acknowledgments

We thank Dr. S. Jaharul Haque for careful reading of the article and helpful comments. We are grateful to Drs. Catherine Chang and Ta Yuan Chang for the gift of SOAT2 antibody.

Grant Support

This work was supported by NIH/NINDS NS072838 (D. Guo) and NS079701 (D. Guo), American Cancer Society Research Scholar Grant *RSG-14-228-01–CSM* (D. Guo), K08 CA155764 (C. Horbinski), OSUCCC start-up funds (D. Guo), and OSU Neuroscience Core MRI pilot grant (D. Guo).

The costs of publication of this article were defrayed in part by the payment of page charges. This article must therefore be hereby marked *advertisement* in accordance with 18 U.S.C. Section 1734 solely to indicate this fact.

Received December 8, 2015; revised May 6, 2016; accepted May 27, 2016; published OnlineFirst June 8, 2016.

References

1. Menendez JA, Lupu R. Fatty acid synthase and the lipogenic phenotype in cancer pathogenesis. Nat Rev Cancer 2007;7:763–77.
2. Guo D, Bell EH, Chakravarti A. Lipid metabolism emerges as a promising target for malignant glioma therapy. CNS Oncol 2013; 2:289–99.
3. Guo D. SCAP links glucose to lipid metabolism in cancer cells. Mol Cell Oncol 2016;3.
4. Guo D, Reinitz F, Youssef M, Hong C, Nathanson D, Akhavan D, et al. An LXR agonist promotes GBM cell death through inhibition of an EGFR/AKT/SREBP-1/LDLR-dependent pathway. Cancer Discov 2011; 1:442–56.
5. Guo D, Prins RM, Dang J, Kuga D, Iwanami A, Soto H, et al. EGFR signaling through an Akt-SREBP-1-dependent, rapamycin-resistant pathway sensitizes glioblastomas to antilipogenic therapy. Sci Signal 2009;2:ra82.
6. Guo D, Bell EH, Mischel P, Chakravarti A. Targeting SREBP-1-driven lipid metabolism to treat cancer. Curr Pharm Des 2014; 20:2619–26.
7. Guo D, Hildebrandt IJ, Prins RM, Soto H, Mazzotta MM, Dang J, et al. The AMPK agonist AICAR inhibits the growth of EGFRvIII-expressing glioblastomas by inhibiting lipogenesis. Proc Natl Acad Sci U S A 2009;106:12932–7.
8. Wen PY, Kesari S. Malignant gliomas in adults. N Engl J Med 2008; 359:492–507.
9. Cheng C, Ru P, Geng F, Liu J, Yoo JY, Wu X, et al. Glucose-mediated N-glycosylation of SCAP is essential for SREBP-1 activation and tumor growth. Cancer Cell 2015;28:1–13.
10. Goldstein JL, DeBose-Boyd RA, Brown MS. Protein sensors for membrane sterols. Cell 2006;124:35–46.
11. Horton JD, Goldstein JL, Brown MS. SREBPs: Activators of the complete program of cholesterol and fatty acid synthesis in the liver. J Clin Invest 2002;109:1125–31.
12. Horton JD, Shah NA, Warrington JA, Anderson NN, Park SW, Brown MS, et al. Combined analysis of oligonucleotide microarray data from transgenic and knockout mice identifies direct SREBP target genes. Proc Natl Acad Sci U S A 2003;100:12027–32.

13. Radhakrishnan A, Goldstein JL, McDonald JG, Brown MS. Switch-like control of SREBP-2 transport triggered by small changes in ER cholesterol: A delicate balance. Cell Metab 2008;8:512–21.
14. Walther TC, Farese RVJr. The life of lipid droplets. Biochim Biophys Acta 2009;1791:459–66.
15. Chang TY, Chang CC, Ohgami N, Yamauchi Y. Cholesterol sensing, trafficking, and esterification. Annu Rev Cell Dev Biol 2006;22:129–57.
16. Oelkers P, Behari A, Cromley D, Billheimer JT, Sturley SL. Characterization of two human genes encoding acyl coenzyme A:cholesterol acyltransferase-related enzymes. J Biol Chem 1998;273:26765–71.
17. Lee JY, Carr TP. Dietary fatty acids regulate acyl-CoA:cholesterol acyltransferase and cytosolic cholesteryl ester hydrolase in hamsters. J Nutr 2004;134:3239–44.
18. Chang CC, Sakashita N, Ornvold K, Lee O, Chang ET, Dong R, et al. Immunological quantitation and localization of ACAT-1 and ACAT-2 in human liver and small intestine. J Biol Chem 2000;275:28083–92.
19. Guo D, Cloughesy TF, Radu CG, Mischel PS. AMPK: A metabolic checkpoint that regulates the growth of EGFR activated glioblastomas. Cell Cycle 2010;9:211–2.
20. Dif N, Euthine V, Gonnet E, Laville M, Vidal H, Lefai E. Insulin activates human sterol-regulatory-element-binding protein-1c (SREBP-1c) promoter through SRE motifs. Biochem J 2006;400:179–88.
21. Huang HS, Nagane M, Klingbeil CK, Lin H, Nishikawa R, Ji XD, et al. The enhanced tumorigenic activity of a mutant epidermal growth factor receptor common in human cancers is mediated by threshold levels of constitutive tyrosine phosphorylation and unattenuated signaling. J Biol Chem 1997;272:2927–35.
22. Han J, Chu J, Keung Chan W, Zhang J, Wang Y, Cohen JB, et al. CAR-engineered NK cells targeting wild-type EGFR and EGFRvIII enhance killing of glioblastoma and patient-derived glioblastoma stem cells. Sci Rep 2015;5:11483.
23. Wojton J, Meisen WH, Jacob NK, Thorne AH, Hardcastle J, Denton N, et al. SapC-DOPS-induced lysosomal cell death synergizes with TMZ in glioblastoma. Oncotarget 2014;5:9703–9.
24. Uchida H, Marzulli M, Nakano K, Goins WF, Chan J, Hong CS, et al. Effective treatment of an orthotopic xenograft model of human glioblastoma using an EGFR-retargeted oncolytic herpes simplex virus. Mol Ther 2013;21:561–9.
25. Singh R, Kaushik S, Wang Y, Xiang Y, Novak I, Komatsu M, et al. Autophagy regulates lipid metabolism. Nature 2009;458:1131–5.
26. Nohturfft A, Brown MS, Goldstein JL. Topology of SREBP cleavage-activating protein, a polytopic membrane protein with a sterol-sensing domain. J Biol Chem 1998;273:17243–50.
27. Boxer MB, Shen M, Zhang Y, Liu L, Auld DS, Beller M. Modulators of lipid storage. Bethesda (MD):Probe Reports from the NIH Molecular Libraries Program; 2010.
28. Chang TY, Chang CC, Lin S, Yu C, Li BL, Miyazaki A. Roles of acyl-coenzyme A:cholesterol acyltransferase-1 and -2. Curr Opin Lipidol 2001;12:289–96.
29. Gao J, Aksoy BA, Dogrusoz U, Dresdner G, Gross B, Sumer SO, et al. Integrative analysis of complex cancer genomics and clinical profiles using the cBioPortal. Sci Signal 2013;6:pl1.
30. Cerami E, Gao J, Dogrusoz U, Gross BE, Sumer SO, Aksoy BA, et al. The cBio cancer genomics portal: an open platform for exploring multidimensional cancer genomics data. Cancer Discov 2012;2:401–4.
31. Lee HT, Sliskovic DR, Picard JA, Roth BD, Wierenga W, Hicks JL, et al. Inhibitors of acyl-CoA: cholesterol O-acyl transferase (ACAT) as hypocholesterolemic agents. CI-1011: an acyl sulfamate with unique cholesterol-lowering activity in animals fed noncholesterol-supplemented diets. J Med Chem 1996;39:5031–4.
32. Burnett JR, Wilcox LJ, Telford DE, Kleinstiver SJ, Barrett PH, Newton RS, et al. Inhibition of ACAT by avasimibe decreases both VLDL and LDL apolipoprotein B production in miniature pigs. J Lipid Res 1999;40:1317–27.
33. Tardif JC, Gregoire J, L'Allier PL, Anderson TJ, Bertrand O, Reeves F, et al. Effects of the acyl coenzyme A:cholesterol acyltransferase inhibitor avasimibe on human atherosclerotic lesions. Circulation 2004;110:3372–7.
34. Bemlih S, Poirier MD, El Andaloussi A. Acyl-coenzyme A: cholesterol acyltransferase inhibitor Avasimibe affect survival and proliferation of glioma tumor cell lines. Cancer Biol Ther 2010;9:1025–32.
35. Paillasse MR, de Medina P, Amouroux G, Mhamdi L, Poirot M, Silvente-Poirot S. Signaling through cholesterol esterification: A new pathway for the cholecystokinin 2 receptor involved in cell growth and invasion. J Lipid Res 2009;50:2203–11.
36. Wojton J, Chu Z, Mathsyaraja H, Meisen WH, Denton N, Kwon CH, et al. Systemic delivery of SapC-DOPS has antiangiogenic and antitumor effects against glioblastoma. Mol Ther 2013;21:1517–25.
37. Ikeda Y, Yamamoto J, Okamura M, Fujino T, Takahashi S, Takeuchi K, et al. Transcriptional regulation of the murine acetyl-CoA synthetase 1 gene through multiple clustered binding sites for sterol regulatory element-binding proteins and a single neighboring site for Sp1. J Biol Chem 2001;276:34259–69.
38. Magana MM, Lin SS, Dooley KA, Osborne TF. Sterol regulation of acetyl coenzyme A carboxylase promoter requires two interdependent binding sites for sterol regulatory element binding proteins. J Lipid Res 1997;38:1630–8.
39. Griffiths B, Lewis CA, Bensaad K, Ros S, Zhang Q, Ferber EC, et al. Sterol regulatory element binding protein-dependent regulation of lipid synthesis supports cell survival and tumor growth. Cancer Metab 2013;1:3.
40. Williams KJ, Argus JP, Zhu Y, Wilks MQ, Marbois BN, York AG, et al. An essential requirement for the SCAP/SREBP signaling axis to protect cancer cells from lipotoxicity. Cancer Res 2013;73:2850–62.
41. Maher EA, Marin-Valencia I, Bachoo RM, Mashimo T, Raisanen J, Hatanpaa KJ, et al. Metabolism of [U-(13) C]glucose in human brain tumors in vivo. NMR Biomed 2012;25:1234–44.
42. Ru P, Williams TM, Chakravarti A, Guo D. Tumor metabolism of malignant gliomas. Cancers (Basel) 2013;5:1469–84.
43. van Meer G, Voelker DR, Feigenson GW. Membrane lipids: where they are and how they behave. Nat Rev Mol Cell Biol 2008;9:112–24.
44. Ridsdale A, Denis M, Gougeon PY, Ngsee JK, Presley JF, Zha X. Cholesterol is required for efficient endoplasmic reticulum-to-Golgi transport of secretory membrane proteins. Mol Biol Cell 2006;17:1593–605.
45. Lange Y. Disposition of intracellular cholesterol in human fibroblasts. J Lipid Res 1991;32:329–39.
46. Hirayama A, Kami K, Sugimoto M, Sugawara M, Toki N, Onozuka H, et al. Quantitative metabolome profiling of colon and stomach cancer microenvironment by capillary electrophoresis time-of-flight mass spectrometry. Cancer Res 2009;69:4918–25.
47. Gullino PM, Grantham FH, Courtney AH, Losonczy I. Relationship between oxygen and glucose consumption by transplanted tumors in vivo. Cancer Res 1967;27:1041–52.
48. Schulze RJ, Weller SG, Schroeder B, Krueger EW, Chi S, Casey CA, et al. Lipid droplet breakdown requires dynamin 2 for vesiculation of autolysosomal tubules in hepatocytes. J Cell Biol 2013;203:315–26.
49. Tuominen VJ, Ruotoistenmaki S, Viitanen A, Jumppanen M, Isola J. ImmunoRatio: A publicly available web application for quantitative image analysis of estrogen receptor (ER), progesterone receptor (PR), and Ki-67. Breast Cancer Res 2010;12:R56.